Integrated-Optical Single-Sideband Modulator and Phase Shifter

FRED HEISMANN AND REINHARD ULRICH

Abstract—A scheme of spatially weighted coupling between two waveguide modes is proposed in which the weights form an electrooptically induced periodic coupling structure that can be moved at variable speeds forward or backward along the guide. The device can operate as an optical phase shifter with unlimited phase range, as a single-sideband amplitude modulator or frequency shifter, or as a polarization transformer.

Introduction

Integrated optical modulators for phase, amplitude, and polarization are expected to find important applications in fiber-optic communication systems and fiber-optic sensors. Here we propose a novel type of modulator. Basically, it is a phase shifter with unlimited range of phase shift μ. Therefore, it may be used in fiber-optic and integrated-optic interferometric sensors [1] to compensate even the largest phase changes which are to be measured. By operating the proposed device with a time-linear phase shift $\mu = \Omega t$, it may also serve as a single-sideband (SSB) modulator, with modulation frequencies ranging from zero up to 10^8–10^9 Hz. Such a frequency shifting is useful in interferometric sensors to convert the optical phase shift to be measured into the low-frequency electronic phase of the detected signal [2], [3]. Finally, the device proposed here may be used as a general polarization transformer. It can convert the fluctuating state of polarization, arriving at the end of a long single-mode fiber-optic transmission line, into any other polarization state required for further processing [4], [5].

Principle of Operation

The principle of the new modulator may be described as spatially weighted coupling between two nonsynchronous waves. In Fig. 1 the two modes indicated may be propagating in two separate (noncoupled) waveguides or they may represent two different modes of a single waveguide. Suppressing a common time factor $\exp(-i\omega t)$, their amplitudes are $a_j(x) \exp(i\beta_j x)$ with $j = 1, 2$, and we assume $\beta_1 > \beta_2$. At some location x_1 the two waves are coupled by a discrete perturbation, characterized by a normalized coupling coefficient κ_1. A wave of unit amplitude is launched into mode 1 at $x = 0$. It propagates with propagation constant β_1 up to the coupling point x_1, where mode 2 becomes excited with amplitude $i\kappa_1$. In that mode the light propagates further with β_2 down to the end of the modulator at $x = L$. There, the amplitude of mode 2, relative to mode 1, is $a_2 = i\kappa_1 \exp(ix_1\Delta\beta)$, where we abbreviated $\Delta\beta = \beta_1 - \beta_2$.

Manuscript received September 9, 1981; revised November 23, 1981.
The authors are with the Technische Universität, Hamburg-Harburg, West Germany.

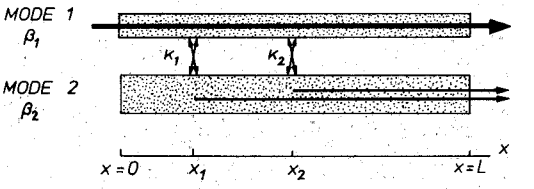

Fig. 1. Schematic representation of spatially weighted coupling between two nonsynchronous waveguide modes.

This consideration shows that the output phase of a_2 depends linearly on the location x_1 of the perturbation. In principle we could vary, therefore, the phase shift $x_1\Delta\beta$ by physically moving the perturbation. Instead, we achieve a variable phase shift here by providing a second perturbation of strength κ_2 at a position x_2 and by then varying the weights κ_1 and κ_2 of the two perturbations. In effect, this moves the centroid of the resulting total perturbation. A suitable separation of the two coupling locations is

$$l_1 \equiv x_2 - x_1 = \Lambda/4 \tag{1}$$

where $\Lambda = 2\pi/\Delta\beta$ denotes the beat length of the two modes. The weights of the couplers are chosen as follows.

$$\kappa_1 = \kappa \cos\mu$$
$$\kappa_2 = \kappa \sin\mu. \tag{2}$$

In practice, coupling with such weights can be realized electrooptically by a pair of electrodes, with applied voltages proportional to κ_1 and κ_2, as will be explained below. Assuming $|\kappa| \ll 1$, we may ignore the perturbations of wave 1 at x_1 and of wave 2 at x_2, and we find at the output

$$a_2 = i\kappa_1 \exp(ix_1\Delta\beta) + i\kappa_2 \exp(ix_2\Delta\beta)$$
$$= i\kappa \exp(ix_1\Delta\beta + i\mu). \tag{3}$$

We recognize that the output phase is shifted simply through the angle $\mu = \arctan(\kappa_2/\kappa_1)$ defined by the weights in (2). By appropriately varying these weights, the shift angle μ can be increased or decreased essentially without limits. By use of the two-phase control according to (2), the shift is continuous at all values of μ, free of the discontinuities and associated spurious sidebands of serrodyne and other pulsed modulations schemes [6].

Cascaded Couplers

As described, the modulation scheme works only in the limit of weak coupling $|\kappa| \ll 1$. To achieve a large or even complete transfer of optical power to wave 2, a large number N (typically $N \gtrsim 10$) of identical pairs (κ_1, κ_2) of weighted couplers is cascaded, as indicated in Fig. 2. A coherent addition of the contributions from all pairs results if the spatial

0018-9480/82/0400-0613$00.75

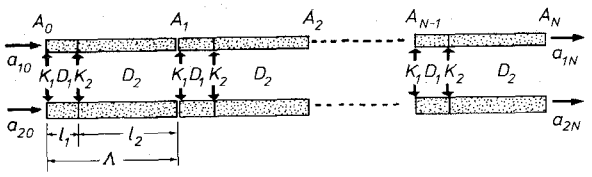

Fig. 2. Representation of N cascaded couplers.

period of this arrangement is chosen equal to the beat length of the two modes, or an integer multiple thereof.

$$l_1 + l_2 = q\Lambda, \quad q = 1, 2, 3 \cdots. \tag{4}$$

Here, l_1 and l_2 denote the distances between consecutive couplers, as shown in Fig. 2. Discussing here only the simplest case $q = 1$, we obtain from (1) and (4) the distance $l_2 = 3\Lambda/4$. The modulation signals (κ_1, κ_2) are applied to all pairs in parallel, requiring only two control voltages. In this way the coupling weights κ_j form a pattern of periodicity Λ and spatial phase μ. By variation of μ, this pattern can be moved forward or backward along the guide.

In analyzing this arrangment we must account for both directions $(1 \leftrightarrow 2)$ of coupling. We denote the amplitudes at the end of the mth section as $a_{j,m}$ and we combine $a_{1,m}$ with $a_{2,m}$ into a column vector A_m. The vectors at output and input of the mth section are related then by a unitary transfer matrix $\boldsymbol{T}$.

$$A_m = \boldsymbol{T} A_{m-1} \tag{5}$$

$$\boldsymbol{T} = \boldsymbol{D}_2\boldsymbol{K}_2\boldsymbol{D}_1\boldsymbol{K}_1 \tag{6}$$

$$\boldsymbol{D}_j = \begin{pmatrix} \exp i\delta_j & 0 \\ 0 & \exp(-i\delta_j) \end{pmatrix} \tag{7}$$

$$\boldsymbol{K}_j = \begin{pmatrix} (1-\kappa_j^2)^{1/2} & i\kappa_j \\ i\kappa_j & (1-\kappa_j^2)^{1/2} \end{pmatrix}. \tag{8}$$

The matrix $\boldsymbol{D}_j$ represents the phase delay difference

$$2\delta_j = l_j \Delta\beta \tag{9}$$

which is accumulated between the two waves when they propagate uncoupled along a distance l_j. According to our choice of l_1 and l_2 we have $2\delta_1 = \pi/2$ for the propagation from κ_1 to κ_2, and $2\delta_2 = 3\pi/2$ for propagation from κ_2 to the subsequent κ_1. The average common phase delay $(\beta_1 + \beta_2)l_j/2$ of the two waves between the beginning and end of l_j is omitted from our equations to permit a more symmetric notation. The matrix $\boldsymbol{K}_j$ represents the localized coupling by the perturbation κ_j.

The overall transfer matrix of the arrangement of N sections, relating the output vector A_N to the input vector A_o, is $\boldsymbol{T}^N$, the Nth power of $\boldsymbol{T}$.

$$A_N = \boldsymbol{T}^N A_o. \tag{10}$$

In the Appendix we show that

$$\boldsymbol{T}^N = (-1)^N [\boldsymbol{R}_N + (1/N)\boldsymbol{S}_N(\kappa)] + \boldsymbol{O}(1/N) \tag{11}$$

$$\boldsymbol{R}_N = \begin{pmatrix} \cos N\kappa & i\exp(-i\mu)\sin N\kappa \\ i\exp(i\mu)\sin N\kappa & \cos N\kappa \end{pmatrix}. \tag{12}$$

Equation (11) is the result of a series expansion in powers of the small quantity κ. The matrix $\boldsymbol{R}_N$ contains the leading terms in the limit of large N, assuming a finite value for the product $N\kappa$. The first-order deviations are expressed by the matrix $\boldsymbol{S}_N$, and $\boldsymbol{O}(1/N)$ contains terms of order N^{-2} and higher. We can discuss now various operating modes of the N-section coupler. To show first the basic performance of the device, we postulate here $N \gg 1$ so that the overall transfer matrix becomes $\pm\boldsymbol{R}_N$.

Phase Modulation

The coupler operates as a lossless phase shifter if we choose the magnitude of the voltages controlling κ_1 and κ_2 so that $N\kappa = \pi/2$. The transfer matrix (12) simplifies to

$$\boldsymbol{R}_N = \begin{pmatrix} 0 & i\exp(-i\mu) \\ i\exp(i\mu) & 0 \end{pmatrix}. \tag{13}$$

This means that the optical input signals into modes 1 and 2 of the first section are completely interchanged at the output of the last section, with their phases shifted through the angle μ. Any positive or negative phase shift μ can be realized by the choice of κ_1 and κ_2 according to (2).

Frequency Modulation

Frequency shifting or modulation of the output signal is obtained in essentially the same way by using a sinusoidal, time-periodic drive voltage for the couplers κ_1, and by driving the couplers κ_2 in quadrature phase.

$$\kappa_1 = \kappa \cos \Omega t$$

$$\kappa_2 = \kappa \sin \Omega t. \tag{14}$$

Choosing again $N\kappa = \pi/2$, the N-section coupler remains continuously in the "crossed" state, but its output signals are downshifted $(1 \rightarrow 2$ coupling) or upshifted $(2 \rightarrow 1$ coupling) in their absolute frequencies by $\Omega/2\pi$. This operation is equivalent to the shift produced by an acoustooptic Bragg modulator. In contrast to the modulation by a traveling acoustic wave, however, an electrooptic implementation of our coupler permits variation of the offset frequency from some maximum frequency $\Omega_{\max}$ all the way down to $\Omega = O$ and up to $\Omega = -\Omega_{\max}$. The frequency limit $\Omega_{\max}$ will presumably be determined only by the electronic circuits (phase shifters) supplying the control voltages. Thus, it may well be in the 10^8–10^9 Hz range.

SSB Amplitude Modulation

Employing control voltages as above, but of variable amplitude

$$\kappa = \bar{\kappa} + \tilde{\kappa}(t) \tag{15}$$

the device can also act as an SSB amplitude modulator. An optimum operating point is $N\bar{\kappa} = \pi/4$. It provides a 3 dB "bias" transfer between modes 1 and 2 and a linear modulation characteristic for small modulation signals $|\tilde{\kappa}| \ll \bar{\kappa}$. As before, the $1 \rightarrow 2$ coupled signal is the lower sideband, and $2 \rightarrow 1$ yields the upper one.

Polarization Conversion

This mode of operation requires implementation of the device in the form of a stripe waveguide in which the waves 1 and 2 propagate in orthogonal polarizations of the fundamental mode. In the example discussed below, a_1 is the amplitude of the TE_0 mode, and a_2 of the TM_0 mode. The vectors A_m then have the meaning of Jones vectors, which we write in the form

$$A_m = \begin{pmatrix} \cos\theta_m \\ \exp(i\delta_m) \cdot \sin\theta_m \end{pmatrix}. \tag{16}$$

Accordingly, the matrix $\boldsymbol{T}^N$ can now be interpreted as an electronically controllable Jones matrix, converting the input polarization state A_o into an output state A_N. A linear input state of azimuth θ_o is characterized, for example by $\delta_o = O$. Operating on such a state A_o with the Jones matrix (12) specialized to $\mu = \pi/2$, yields an output state which is linear, too ($\delta_N = O$), but whose azimuth θ_N is rotated through $N\kappa$.

$$\theta_N = \theta_o - N\kappa. \tag{17}$$

More generally, it is possible with the N-section coupler to convert [5] any given elliptical input state into any desired output state by properly adjusting both control parameters μ and $N\kappa$. For example, the general input state A_o is converted to a pure TE_0 output mode ($\theta_N = 0$) if we choose

$$\mu = \delta_o + \pi/2$$
$$N\kappa = \theta_o. \tag{18}$$

Although this transformation with only two adjustable parameters (κ, μ) is not the most general polarization transformation, it is sufficient for the stabilization of output polarization [4], allowing arbitrary fluctuations of the input state. Compared to the polarization transformer of [5], the one discussed here has the advantage of an unlimited range, permitting continuous operation without need for occasional reset cycles [4].

Coupler with Finite N

The preceding discussions dealt only with the limit $N \to \infty$, where $\boldsymbol{T}^N$ is represented by $\boldsymbol{R}_N$. In practice, a finite N must be used, and it is of interest to determine the resulting deviations in the modulation. It is sufficient to consider here only the application as a phase shifter because it exhibits the largest deviations. They are represented in (11) by the matrix $\boldsymbol{S}_N$ which is specified in the Appendix. Inserting there into (26) the maximum applicable value $N\kappa = \pi/2$, it can be shown that for $N \geqslant 9$ the absolute value of all components of $\boldsymbol{S}_N$ remains below 0.82. With that number, (11) permits the following estimate of the maximum possible deviations of the output wave due to the finiteness of N. For an input wave A_o of unit power ($|a_{10}|^2 + |a_{20}|^2 = 1$), the output wave A_N has also unit power, but both amplitudes $|a_{1N}|$ and $|a_{2N}|$ may deviate from their ideal ($N \to \infty$) values by no more than $0.82/N$. The equivalent error in the phase shift angle is of the order $0.82/N$ rad. For example, to keep the amplitude error below 10 percent of the maximum amplitude and the phase error below 0.1 rad, we must choose $N \geqslant 9$. Of course, this estimate applies only to the errors intrinsic in cascading a finite number of couplers. Additional errors may result from fabricational imperfections like irregular drift distances l_j.

The finite length of a real coupler also determines its optical bandwidth. Like in other birefringent devices [5], the relative bandwidth is $\Delta\lambda/\lambda \approx \Lambda/2L$, where L is the total device length.

Implementation

The design of the proposed coupler is shown schematically in Fig. 3. Waves 1 and 2 propagate as TE_0 and TM_0 modes, respectively, along the y direction of a stripe waveguide diffused into an x-cut $LiNbO_3$ substrate. The difference of their propagation constants is $\Delta\beta \approx 2\pi/\lambda\Delta n$, mainly determined by the birefringence Δn of the crystal. For $\lambda = 0.6\ \mu$m, for example [7], $\Lambda = 7\ \mu$m.

Coupling between the two modes is effected electrooptically by interdigital electrodes, as in the TE $\leftrightarrow$ TM mode converter of Alferness and Buhl [7]. The basic coupling mechanism is the off-diagonal component ϵ_{13} of the dielectric tensor of the crystal, induced by the modulating voltages underneath the edges of the control electrodes and adjacent ground electrode. As the relevant x-component of the inducing field has opposite directions at neighboring edges, the optimum width of the fingers and gaps of the electrode pattern is $\sim\Lambda/4$. Each control electrode combined with the neighboring edges of the ground electrode plays the role of one of the couplers κ_j discussed above. Although these couplers are not localized, the theory given remains applicable. To accommodate these extended couplers, both separations l_j had to be increased by Λ in the design of Fig. 3(a), as compared to the basic concept of Fig. 2. Therefore, $2\delta_1 = 5\pi/2$ and $2\delta_2 = 7\pi/2$, here, and the period length is 3Λ.

The coupling factor κ of a single control electrode (finger pair of separation $\Lambda/2$) can be expressed in the form [7]

$$\kappa = \alpha\pi n^3 r_{51} \frac{V}{d}\frac{\Lambda}{\lambda}. \tag{19}$$

Here, n is an average index of the guide, $r_{51} \sim 28 \cdot 10^{-12}$ m/V is a component of the electrooptic tensor of the crystal, V is the peak voltage applied to the electrodes, d is the width of the interelectrode gap, and λ is the wavelength in free space. The dimensionless factor α, ranging between 0 and 1, is the normalized overlap integral of the field under the electrodes with the product of the TE_0 and TM_0 field distributions. A realistic value [7] for the interdigital electrode pattern is $\alpha = 0.16$.

The weighting of the coupling as required by (2) is achieved by applying modulated voltages $V_1 = V\cos\mu$ and $V_2 = V\sin\mu$ to the control electrodes κ_1 and κ_2, respectively. Using a peak voltage of, e.g., $V = 10$ V, $\lambda = 0.6\ \mu$m, and $\Lambda = 7\ \mu$m, we find $\kappa = 0.011$, and the phase shifter requires $N \approx 150$ periods. As one period occupies 3Λ in the pattern of Fig. 3(a), the actual length of such a coupler would be $450\ \Lambda \approx 3$ mm.

Although the electrode arrangement Fig. 3(a) has the advantage of a large N, it requires isolated crossings of the electric connections to N control electrodes. This problem can be

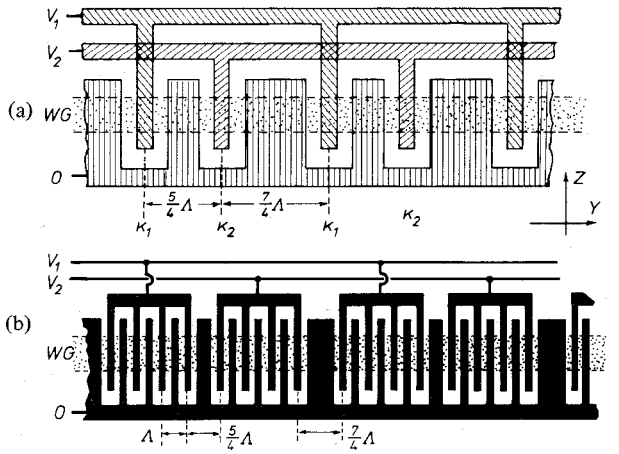

Fig. 3. Electrode patterns for electrooptic implementation of phase shifter. WG-waveguide. (a) Simple arrangement according to Fig. 2 with 3 Λ period. (b) Arrangement of groups ($M = 4$) of control electrodes with reduced number of intersections and reduced overall length.

reduced considerably by rearranging those connections according to Fig. 3(b). Here, groups of M successive control electrodes at spacings Λ are connected (without line crossings) in parallel and form one of the couplers κ_j mentioned above. Two groups form one period (κ_1, κ_2), with extra spacings l_j of alternatingly $\Lambda/4$ and $3\,\Lambda/4$ between neighboring groups. The coupling factor of each group is $\kappa_M = M\kappa$, and the number of groups required for the phase shifter is $N_M = \pi/2\kappa_M = N/M$. Thus, the total number of control electrodes in Fig. 3(b) is the same as in Fig. 3(a), but the number of isolated crossings has been reduced by the factor M. This factor is limited by the requirement that N_M must remain large enough to avoid the mentioned distortions of the modulation characteristic. The -20 dB limit is guaranteed with $N_M = 10$ and $M = 15$. This requires only 9 line crossings, realizable, e.g., with bond wires. Moreover, as most control electrodes are spaced here by Λ, the overall length of the pattern Fig. 3(b) is reduced nearly by a factor of $\frac{2}{3}$ in comparison to Fig. 3(a).

Discussion

We have proposed an electrooptic phase shifter with unlimited phase range. This has been possible, from a systems viewpoint, by the use of two control voltages (V_1, V_2) instead of one. In a simple electrooptic phase shifter the shift angle μ is proportional to the applied voltage and is therefore limited. In the new coupler, however, the two control voltages are 90° out of phase and continuously alternate in their phase-shifting role. This type of control is comparable to the operation of a 2-phase synchronous motor. Extending this comparison, one could even envisage a 3-phase version of our phase shifter, requiring three control voltages offset by 120° and three couplers κ_j separated by equal drift spaces $l_j = \Lambda/3$.

From a microscopic viewpoint, the continuous unlimited phase shift μ is achieved by the scheme of spatially weighted coupling introduced above. This scheme becomes particularly clear when we consider its operation in SSB modulation with $\mu = \Omega t$. In that case coupling is provided by a traveling "wave" of off-diagonal polarizability ϵ_{13}, induced by the electrode pattern. In the basic scheme (Fig. 2) this wave propagates with $\exp(i\Omega t - ix\Delta\beta)$ along the guide. The frequency shift in coupling may be regarded as the result of forward light scattering at this moving perturbation, comparable to a Bragg-reflection at a traveling acoustic wave. In contrast to the acoustic wave, however, the velocity $\Omega/\Delta\beta$ of the ϵ_{13} wave can be varied at will by adjustment of Ω. This wave can even be frozen at any position, the resulting phase shift depending linearly on this position.

In conclusion, the proposed phase shifter combines the advantages of speed and low drive power, characteristic for electrooptic modulation, with the potentials of traveling-wave interaction characteristic for acoustooptic modulation.

Appendix

For a calculation of the overall transfer matrix of an N-section coupler we evaluate (6)-(8) employing a series expansion of the diagonal terms of $\boldsymbol{K}_j$.

$$\boldsymbol{T} = -[\boldsymbol{T}_o - (\kappa^2/2)(\boldsymbol{I} - i \sin 2\mu\, \boldsymbol{J}) + \boldsymbol{O}(\kappa^2)] \tag{20}$$

$$\boldsymbol{T}_o = \begin{pmatrix} 1 & i\kappa \exp(-i\mu) \\ i\kappa \exp(i\mu) & 1 \end{pmatrix} \tag{21}$$

$$\boldsymbol{I} = \begin{pmatrix} 1 & 0 \\ 0 & 1 \end{pmatrix}; \quad \boldsymbol{J} = \begin{pmatrix} 1 & 0 \\ 0 & -1 \end{pmatrix}. \tag{22}$$

The matrix $\boldsymbol{T}_o$, which represents $-\boldsymbol{T}$ in the limit $\kappa \to 0$, is diagonalized by the transformation $\boldsymbol{T}_o = \boldsymbol{U}\boldsymbol{D}_T\boldsymbol{U}^{-1}$ with a unitary matrix $\boldsymbol{U}$.

$$\boldsymbol{U} = \frac{1}{\sqrt{2}} \begin{pmatrix} 1 & -\exp(-i\mu) \\ \exp(i\mu) & 1 \end{pmatrix} \tag{23}$$

$$\boldsymbol{D}_T = \begin{pmatrix} 1 + i\kappa & 0 \\ 0 & 1 - i\kappa \end{pmatrix}. \tag{24}$$

To calculate T^N we use $T_o^N = UD_T^N U^{-1}$ and the following expansion, valid for finite $(N\kappa)$ and $N \gg 1$.

$$(1 \pm i\kappa)^N = [1 + N\kappa^2/2] \exp(\pm iN\kappa) + O(1/N). \quad (25)$$

Combining these equations we obtain (6), and with a lengthy summation procedure

$$S_N(\kappa) = (N^2\kappa^2/2)[R_N - R_{N-1} + i(\sin 2\mu \sin N\kappa/N \sin \kappa)J]. \quad (26)$$

References

[1] D. A. Jackson, A. Dandridge, and S. K. Sheem, "Measurement of small phase shifts using a single-mode optical-fiber interferometer," *Opt. Lett.*, vol. 5, pp. 139–141, 1980.

[2] N. A. Massie, R. D. Nelson, and S. Holly, "High-performance real-time heterodyne interferometry," *Appl. Opt.*, vol. 18, pp. 1797–1803, 1979.

[3] R. F. Cahill and E. Udd, "Phase-nulling fiber-optic laser gyro," *Opt. Lett.*, vol. 4, pp. 93–95, 1979.

[4] R. Ulrich, "Polarization stabilization on single-mode fiber," *Appl. Phys. Lett.*, vol 35, pp. 840–842, 1979.

[5] R. C. Alferness and L. L. Buhl, "Waveguide electro-optic polarization transformer," *Appl. Phys. Lett.*, vol. 38, pp. 655–657, 1981.

[6] R. J. King, *Microwave Homodyne Systems.* Stevanage, UK: Peter Peregrinus Ltd., 1978; and B. Culshaw and M.F.G. Wilson, "Integrated optic frequency shifter modulator," *Electron. Lett.*, vol. 17, pp. 135–136, 1981.

[7] R. C. Alferness and L. L. Buhl, "Electro-optic waveguide TE ↔ TM mode converter with low drive voltage," *Opt. Lett.*, vol. 5, pp. 473–475, 1980.

Fred Heismann was born in Gütersloh, Germany, on January 19, 1955. He received the Diplom. degree in physics from the University of Bielefeld, Bielefeld, Germany, in 1980.

He is currently with the Technische Universität, Hamburg-Harburg, Germany, where his research interest is in the field of optical guided-wave devices.

Mr. Heismann is a member of the American Physical Society.

Reinhard Ulrich was born in Wuppertal, Germany, on February 22, 1935. He received the Diplom-Physiker degree and the Ph.D. degree in physics from the University of Freiburg, i. Br., Germany, in 1962 and 1965, respectively.

In 1967 after postdoctoral research on FIR filters at Ohio State University, Columbus, he joined Bell Laboratories, Holmdel, NJ, where he worked on early problems of integrated optics. From 1972 to 1980 he was with Max-Planck-Institut für Festkörperforschung, Stuttgart, Germany, investigating general problems of optical guided waves. Since 1980 he has been a Professor of Optics and Metrology at the Technische Universität, Hamburg-Harburg, Germany, where he is engaged in research on fiber-optical and integrated-optical sensors

Dr. Ulrich is a member of the Verein Deutscher Elektrotechniker and the Deutsche Gesellschaft für angewandte Optik, and a Fellow of the American Optical Society.

Crosstalk Characteristics of Ti-$LiNbO_3$ Intersecting Waveguides and Their Application as TE/TM Mode Splitters

HIROCHIKA NAKAJIMA, TETSUO HORIMATSU, MEMBER, IEEE, MINORU SEINO, AND IPPEI SAWAKI

Abstract—**Crosstalk characteristics of an intersecting waveguide are presented. Two straight channel waveguides which intersect at an angle of a few degrees on *y*-cut $LiNbO_3$ were fabricated by in-diffusion of Ti. Experimental results show that the crosstalk characteristics are determined by the refractive index change profile and the geometry of intersection associated with guided wave modes. In a special case, a TE/TM mode splitter was obtained by using the intersecting waveguide which provides adequate anisotropy by the change in refractive indices. Splitting ratio was 17 and 14 dB for the TE and TM modes, respectively.**

Manuscript received September 4, 1981; revised November 18, 1981.
The authors are with Fujitsu Laboratories Ltd., Kawasaki, Japan.

I. Introduction

RECENT growth in research concerning planar optical devices has spread to cover a wide range of applications. For example, functional optical devices, such as optical modulators/switches based on directional coupling between two adjacent strip waveguides have been theoretically designed and demonstrated [1]-[3]. On the other hand, experimental results and theoretical analysis on functional devices using *Y*-branch waveguides have also been reported [4], [5]. We have focused our attention on an intersecting waveguide [6], [7] as another useful planar device for functional applications. This

0018-9480/82/0400-0617$00.75